EX/P3-12

Transition Phenomena and Thermal Transport Property in LHD Plasmas with an Electron Internal Transport Barrier

T. Shimozuma1), S. Kubo1), H. Idei2), S. Inagaki1), N. Tamura1), K. Ida1), I. Yamada1), K. Narihara1), S. Muto1), M. Yokoyama1), Y. Yoshimura1), T. Notake3), K. Ohkubo1), T. Seki1), K. Saito1), R. Kumazawa1), T. Mutoh1), T. Watari1)
and LHD Experimental Group

1) National Institute for Fusion Science, 322-6 Oroshi-cho, Toki-city, Gifu 509-5292, Japan
2) Kyushu University, Kasuga, Fukuoka 816-8580, Japan
3) Dept. of Energy Eng. and Sci., Nagoya University, Nagoya 464-8603, Japan

e-mail contact of main author: shimozuma.takashi@LHD.nifs.ac.jp

Abstract. Two kinds of improved core confinement were observed during centrally focused Electron Cyclotron Heating (ECH) into plasmas sustained by Counter (CNTR) and Co Neutral Beam Injections (NBI) in the Large Helical Device (LHD). One shows transition phenomena to the high-electron-temperature state and has a clear electron Internal Transport Barrier (eITB) in CNTR NBI plasma. Another has no clear transition and no ECH power threshold, but shows a broad high temperature profiles with moderate temperature gradient, which indicates the improved core confinement with additional ECH in Co NBI plasma. The electron heat transport characteristics of these plasmas were directly investigated by using the heat pulse propagation excited by Modulated ECH (MECH). The difference of the features could be caused by the existence of the m/n=2/1 rational surface or island determined by the direction of NBI beam-driven current.

1. Introduction

In recent years, many efforts to elucidate the mechanism of improved confinement with internal transport barriers have been extensively made. There are comprehensive review articles for both tokamak [1] and stellarator devices [2]. For stellarator machines, in special, many interesting phenomena have been observed related with intense local heating by electron cyclotron heating (ECH), such as formation of ITBs [3-6], achievement of the electron root [7], the bifurcation phenomena of radial electric field [8] and transient behavior like pulsation [9]. These phenomena are interpreted to be induced by creation of ambipolar radial electric field due to unbalance of electron and ion losses, decrease of electron heat diffusivity under the existence of such electric filed and suppression of turbulence by the shear of radial electric field [2].

In the Large Helical Device (LHD), high electron temperature over 10keV and transition behavior to such state with the formation of ITB have been achieved by means of high power ECH over 2MW and using strongly focused mirror antennas. In experiments, neutral-beam-driven currents modify the profiles of rotational transport $\iota/2\pi$, and two different kinds of improved confinement were observed. In this paper, using the techniques of heat pulse propagation generated by modulated ECH (MECH), we tried to elucidate the mechanisms of realization of these discharges.

This paper is organized as follows. At first the experimental apparatus and configuration are explained in Sec. 2. In Section 3, the feature of ITB plasmas in LHD and the transition phenomena to the high-central-T_e state induced by external perturbations are given. The method and analyzed results of MECH technique for various target plasmas are described in Sec. 4. Finally discussions and summary will be given in Sec. 5

2. Experimental Configuration

LHD is the largest heliotron-type device (l=2, m=10) with superconducting helical coils and poloidal coils. The major and the averaged minor radii of the produced plasmas are typically 3.5m and 0.6m, respectively. The ECH system consists of two 82.7GHz and two 84GHz gyrotrons for fundamental resonance heating, and four 168GHz gyrotrons for second harmonic heating at 3T [10]. In the present experiments 82.7GHz power was injected from the antenna installed in the upper port (upper antenna), 84GHz power was launched from the antenna in the lower port (lower antenna) as shown in Fig.1 (a). The upper and lower antennas are installed in the toroidal section with the vertically elongated cross section. The beam waist radii at the focal point are 15mm in the radial direction for the upper antenna, and 30mm for the lower antenna. The MECH power of 168GHz was injected from upper antenna.

The electron temperature profiles are measured by a Thomson scattering system at about 110 positions in the equatorial plane of the horizontally elongated toroidal section, with a spatial resolution of 20 - 35mm [11]. For T_e measurements with higher time resolution, a multi-channel radiometer system was installed to detect electron cyclotron emission (ECE) at the low magnetic field side (32 channels, spatial resolution: 10 - 70mm) [12].

A schematic of the time sequence in NBI, ECH and pellet injection is illustrated in Fig. 1 (b). The target plasmas were produced by NBI and additional ECH was turned on at the flat top of the discharge in Fig. 1 (b). The typical line-averaged electron density was 0.5 - 0.7×10^{19} m^{-3}. The MECH pulse (50% duty, modulation frequency was 35Hz) was superposed during the ECH pulse. The direction of beam-driven currents was changed by switching the injection direction of NBI.

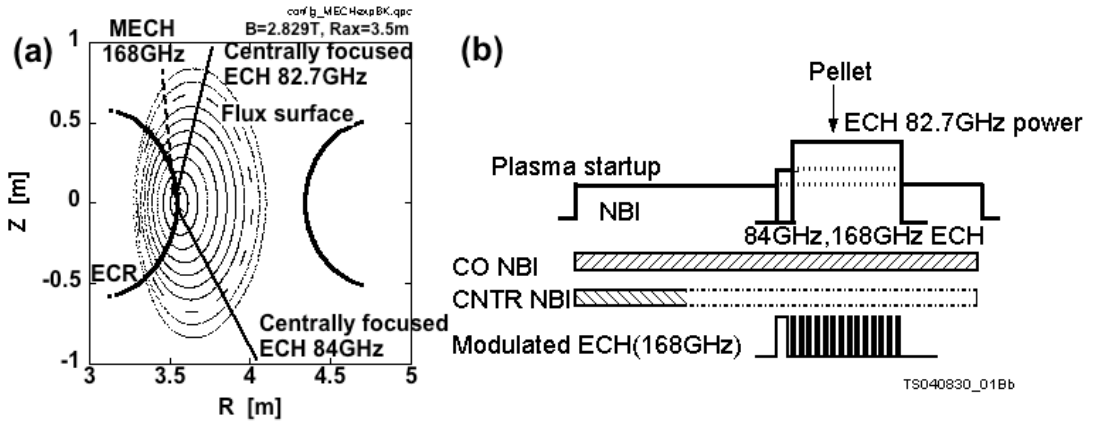

FIG. 1. Experimental configuration is shown in (a) with ECH injection direction. (b) Typical time sequence in NBI, ECH and pellet injection.

3. Feature of Electron ITB and Transition Phenomena Triggered by External Perturbations

Clear formation of an eITB was observed in CNTR NBI sustained plasmas with centrally focused ECH [3]. The electron temperature profile of the plasma shows a clear foot position and a steep gradient around normalized minor radius ρ=0.3. On the formation of the ITB, some transition phenomena to the high-electron-temperature state were observed, which could

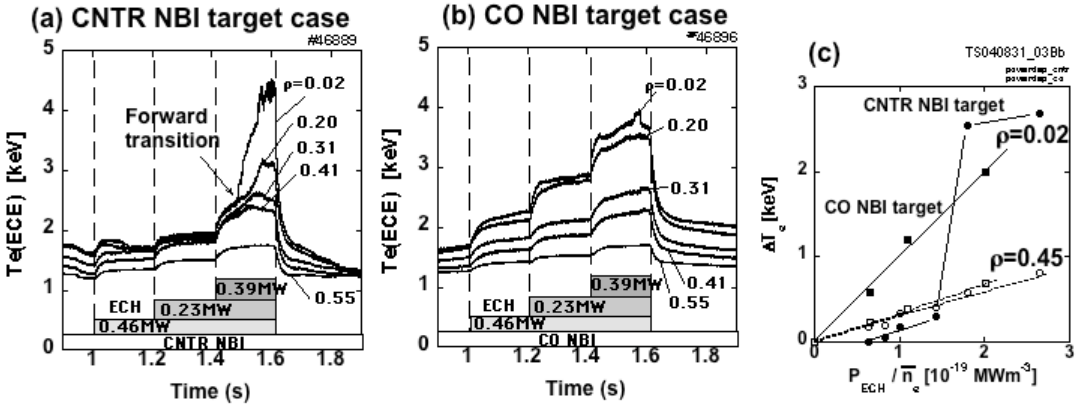

FIG. 2. Electron temperature evolutions for stair-like ECH power injection into (a) CNTR and (b) Co NBI sustained plasmas. Electron temperature increases at the center and periphery are plotted as a function of density-normalized ECH power in (c).

be triggered by the external perturbations, such as additional ECH power, slight density decrease, small pellet injection and so on. To clarify the transition phenomena by additional ECH, injection power was increased in a staircase pattern. Figure 2 (a) and (b) show the time evolution of the electron temperature measured by ECE at several normalized radii, ρ, for the CNTR and Co NBI target plasmas, respectively. There was a clear forward transition to the high-central-T_e state in the only CNTR NBI plasma as shown in Fig. 2 (a). A decay time of the central T_e is longer than one at the periphery and of Co NBI case. The increment of the electron temperature, ΔT_e, at the plasma center by ECH power is plotted in (c) as a function of ECH power normalized by the electron density. Obvious ECH power threshold can be noticed for the case of the CNTR NBI plasma. On the other hand, there is no threshold power in the Co NBI case, and the central T_e increases almost linearly with ECH power and moves to the high-T_e state.

A transition to the high-T_e state could be also induced by slight density decrease. During additional ECH injected into a CNTR NBI sustained plasma, central electron temperature spontaneously built up at latter half of the ECH pulse shown in Fig. 3 (a). The line-averaged

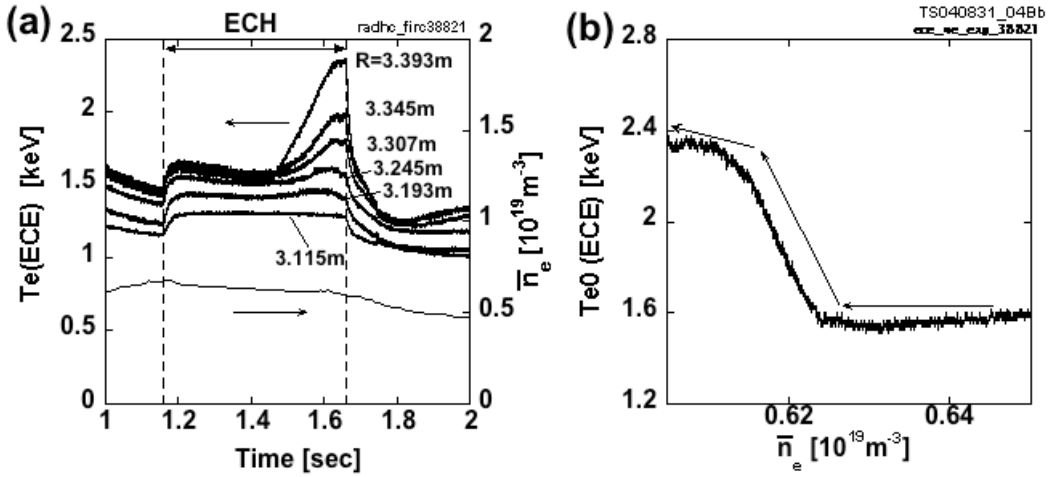

FIG. 3. High-T_e transition induced by a little density decrease. Time evolution of electron temperature measured by ECE is plotted in (a). The central electron temperature is plotted as a function of line-averaged electron density in (b).

electron density gradually decreased during ECH pulse, then the transition happened. In Fig. 3 (b) the central electron temperature T_{e0} is plotted as a function of line-averaged electron density. A little density decrease of 10^{17} m^{-3} led to about 1keV temperature rise. Another high–T_e transition was triggered by small pellet (TESPEL) injection due to edge-plasma cooling as shown in Fig. 4. The CNTR NBI sustained plasma was heated additionally by ECH, though the ECH power level was below the threshold value for transition. After TESPEL injection at 1.645s, central electron temperature up to ρ=0.3 increased after cooling of edge plasma within 3ms. The increase of the line-averaged density was below 1×10^{18} m^{-3} by the pellet injection for this case.

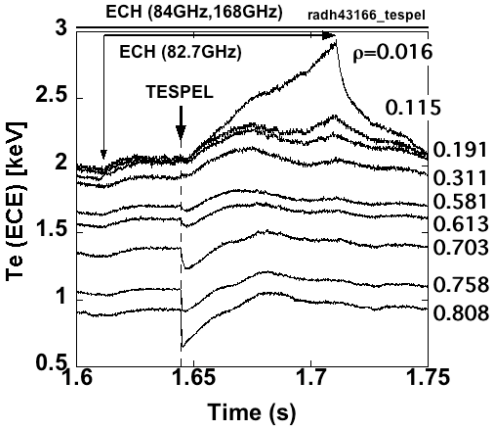

FIG. 4. Transition was triggered by small pellet injection even though ECH power level was below the threshold value for transition.

4. Heat Transport Analysis by Modulated ECH in High T_e Plasmas

Direct observation of the existence of the transport barrier was tried by means of heat pulse propagation excited additional modulated ECH power (168GHz, 0.2MW, 35Hz, and duty 50%). Target plasmas for investigation are NBI reference and NBI plus ECH plasmas. The modulation frequency was precedently optimized for heat pulse propagation in view of the sampling time of ECE and MECH pulse width. Figure 5 (a) shows temperature oscillation measured by ECE at each radial position for a typical CNTR NBI sustained plasma. The scale of the vertical axis is the same for all frames. The maximum amplitude of ΔT_e is about 50eV at ρ=0.02. The Fourier spectrum of the ECE signal at ρ=0.02 is shown in Fig. 5 (b). The peaks

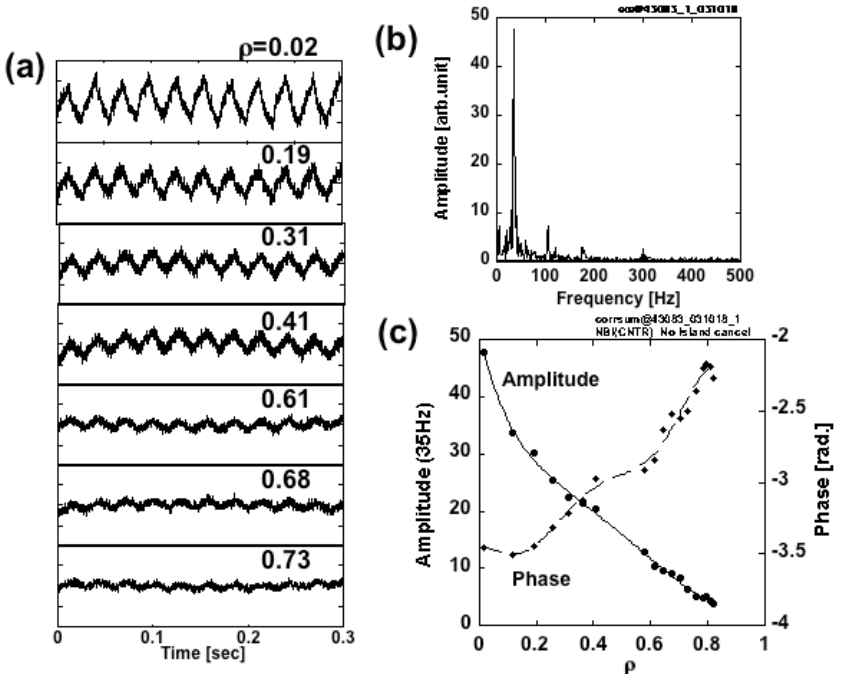

FIG. 5. ECE signal processing excited by MECH. (a) Time evolution of ECE signal at each radial position plotted in the same vertical scale. (b) Fourier spectrum of ECE signal at ρ=0.02. (c) Radial profile of 35Hz component of the frequency spectrum, both amplitude and phase. profiles.

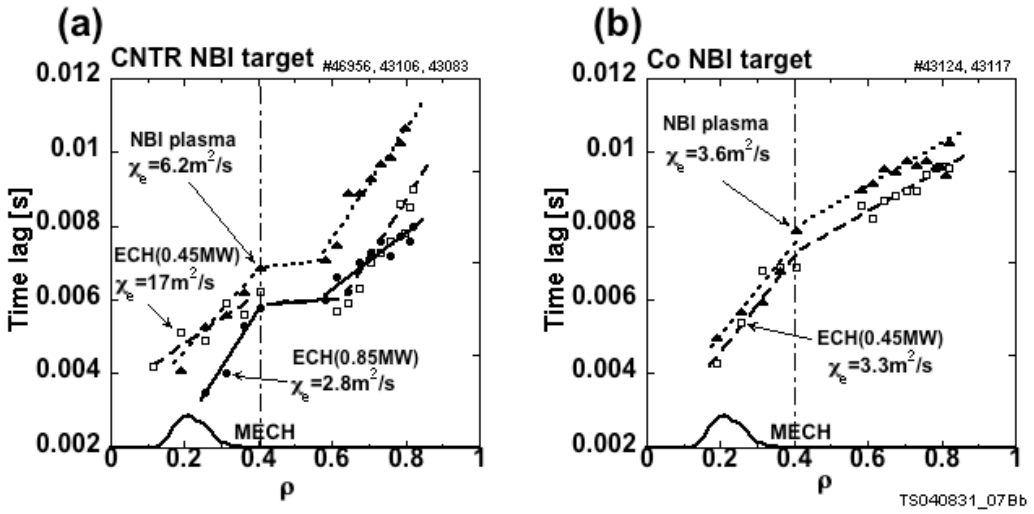

FIG. 6. Time lag of ECE signals from MECH is plotted for normalized minor radius. (a) CNTR NBI sustained plasma, (b) Co NBI case. The closed triangles, open squares and closed circles correspond to the data of NBI reference plasma, NBI plasma with 0.45MW ECH power and NBI plasma with 0.85MW ECH power, respectively. Electron heat diffusivities estimated from heat pulse propagation velocity are also indicated in the figures.

of the fundamental (35Hz), third (105Hz) and fifth harmonics (175Hz) can be identified. The Fourier amplitude and phase of the modulation frequency (35Hz) are plotted in Fig. 5 (c). A time lag of ECE signal rise at each radial position from MECH ON timing is determined by the correlation calculation between each ECE signal and MECH signal, which is defined as follows.

$$Corr(S_{MECH}, S_{ECE})(\rho, t) = \int_{-\infty}^{\infty} S_{MECH}(\tau + t) S_{ECE}(\rho, \tau) d\tau, \quad (1)$$

where $S_{MECH}(t)$ is an MECH signal and $S_{ECE}(\rho,t)$ is a calibrated ECE signal at ρ position.

The time lag that gives the maximum correlation at each position is plotted in Fig. 6, together with power deposition profile of the MECH calculated by a ray tracing code. The incremental electron heat diffusivity, χ_e, is evaluated from the relation, $\chi_e = V^2/(4\pi f_{mod})$, assuming a constant value of χ_e and slab model within ρ=0.4, where V is a propagation velocity of the heat pulse that is calculated from the ratio of the propagation distance and the time lag. The modulation frequency of MECH is denoted by f_{mod}. The evaluated χ_e values are also described in the figure. Remarkable difference of propagation behavior can be noticed between CNTR and Co cases. As shown in Fig. 6 (a), the heat diffusivity in the core region ($\rho < 0.4$) once increased with ECH power injection (0.45MW), and then drastically decreased by injection of more ECH power above the threshold value. This behavior and spatial change of χ_e within ρ=0.4 by the ECH power increase (0.45 to 0.85MW) imply an improved confinement and a barrier structure within ρ=0.4. On the other hand, the heat diffusivity in the Co NBI sustained plasma was not changed so much by superposition of ECH power. Considering additional ECH power, the confinement is not degraded even with ECH power injection. The heat diffusivity normalized by the gyro-Bohm scaling $T_e^{3/2} / B^2$ reduced from 8.0 to 3.8 $m^2 \cdot s^{-1} \cdot keV^{3/2} \cdot T^2$ with the power increase by ECH, which means a kind of improved confinement except an anomalous transport part.

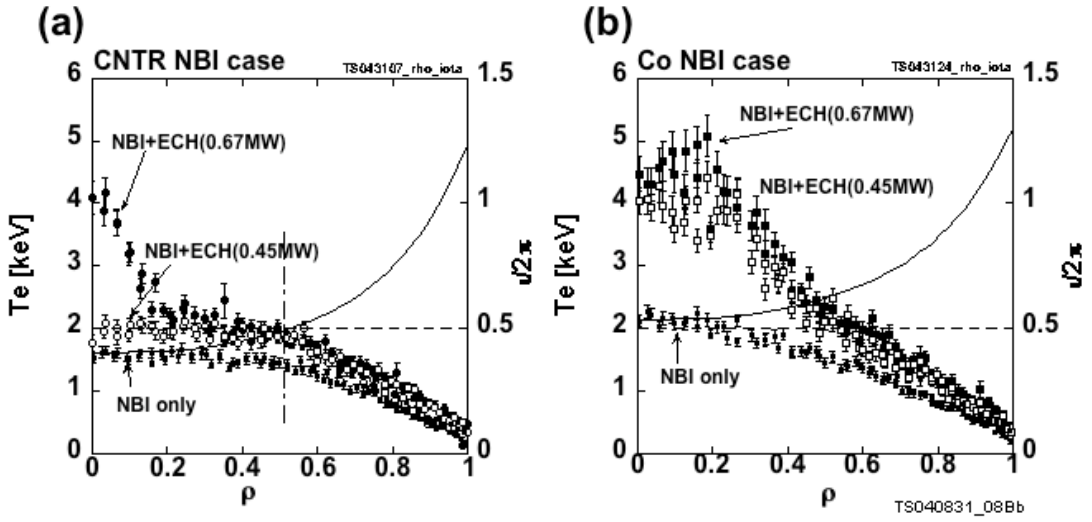

FIG. 7. Electron temperature profiles for NBI, NBI+ECH(0.45MW), NBI+ECH(0.67MW) plasmas. Target plasmas are sustained by (a) CNTR injected and (b) Co injected NBI.

There is a difference in the direction of NBI-driven currents between CNTR and Co injections, i.e., a profile difference of the rotational transform, $\iota/2\pi$. An equilibrium calculation including the beam-driven current shows that a rational surface of $\iota/2\pi=1/2$ exists around the position $\rho=0.5$ for the CNTR case, while no such surface exists in the Co NBI plasma. Figure 7 (a) and (b) shows typical electron temperature profiles for CNTR and Co NBI sustained plasmas with calculated rotational transform profiles. The CNTR NBI-driven current reduces the rotational transform in the core region from the value for the vacuum magnetic field, and $\iota/2\pi=1/2$ appears in the plasma. The flattening of a time lag from $\rho=0.4$ to 0.55 in Fig. 6 (a) suggests the existence of the m/n = 2/1 island where the quick radial propagation can be driven by the fast parallel heat transport on the separatrix of the island.

5. Discussions and Summary

The determining factor of the ITB foot position is one of key factors to elucidate a complex

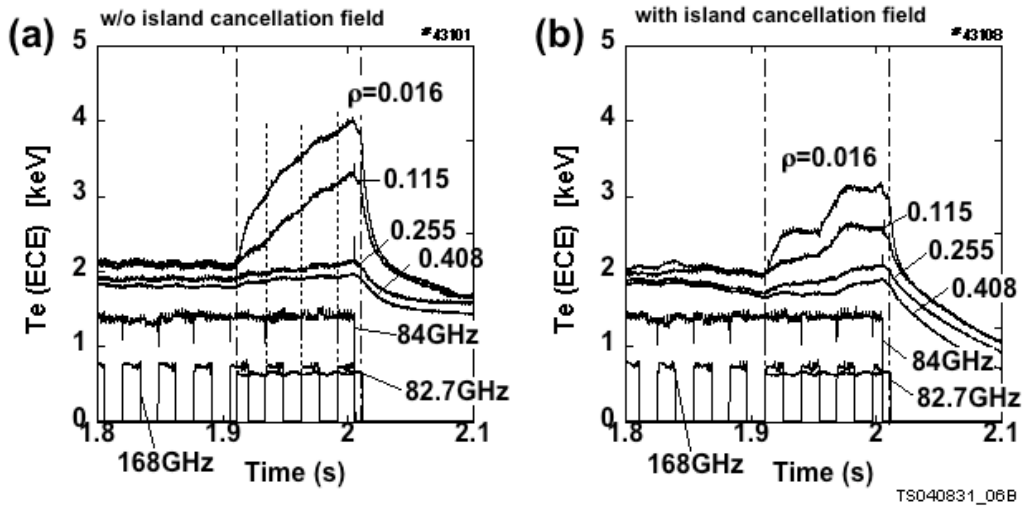

FIG. 8. Effect of the island-cancellation-magnetic-field on the transition to the high-T_e during additional ECH. (a) with island cancellation (b) without cancellation field.

dynamics of barrier formation mechanism. To clarify the effect of existence of 2/1 natural island on the high-T_e transition, a cancellation magnetic field was superposed by means of external perturbation coils. Figure 8 shows the effect of the island cancellation field on the CNTR NBI target plasma during additional ECH injection (a) with the natural island and (b) without the island. Increase of the central electron temperature is large and smooth for the plasma with the island. This experimental evidence assures that the existence of the 2/1 island is a candidate of the triggering mechanism of radial electric field bifurcation [13], and the electric field domain interface could suppress the anomalous transport, resulting in the formation of an ITB [14,15].

On the other hand, in the Co NBI case, the electron heat transport in the core region was not changed, although ECH power was injected into the core region (ρ<0.2). The ambipolarity condition of electron and ion fluxes predicts the existence of positive radial electric field over wide range. The generated radial electric field could improve the core confinement neoclassically except a part of anomalous transport. The neoclassical electron-root plasma seems to be realized in the core region.

In summary, two types of improved core confinement were realized by centrally focused ECH in the NBI-sustained LHD plasmas. These plasmas could be controlled by the injection direction of NBI-driven current. In the CNTR injection case, the temperature profile in the core had a narrow profile and steep temperature gradient, and an electron ITB was established in the core region. Transition behavior to the high-T_e state was sometimes observed, which was triggered by some external perturbations, such as additional ECH power, a little decrease of density, small pellet injection and so on. In the Co NBI case, plasma that had a broad high-T_e profile and moderate temperature gradient was realized. This plasma had no threshold ECH power for transition to high-T_e state. Characteristics of the heat transport in these plasmas were directly measured by heat pulse propagation generated by additional modulated ECH. In special, the formation process of the ITB was investigated. The existence of 2/1 island or low order rational surface may facilitates the transition to high-T_e state and the formation of an ITB with a steep temperature gradient in the CNTR NBI plasmas. On the other hand, in the Co NBI injection plasma, which has a broad high-T_e profile and no clear ECH power threshold, the positive radial electric field (electron-root) could improve core confinement in the neoclassical means, though a part of anomalous heat transport still exists.

References

[1] WOLF, R.C., “Internal transport barriers in tokamak plasmas”, Plasma Phys. Control. Fusion **45** (2003) R1.
[2] FUJISAWA, A., “Experimental studies of structural bifurcation in stellarator plasmas”, **45** (2003) R1.
[3] SHIMOZUMA, T., et al., “Formation of electron internal transport barrier by highly localized electron-cyclotron-resonance heating in the large helical device”, Plasma Phys. Control. Fusion **45** (2003) 1183.
[4] TAKEIRI, Y., et al., “Formation of electron internal transport barrier and achievement of high ion temperature in large helical device”, Phys. Plasmas **10** (2003) 1788.
[5] IDA, K., et al., “Characteristics of electron heat transport of plasma with an electron internal-transport barrier in the large helical device”, Phys. Rev. Lett. **91** (2003) 085003.
[6] ESTRADA, T., et al., “Electron internal transport barrier formation and dynamics in the plasma core of the TJ-II stellarator”, Plasma Phys. Control. Fusion **46** (2004) 277,

[7] MAASSBERG, H., et al., “The neoclassical electron root feature in the Wendelstein-7-AS stellarator”, Phys. Plasmas **7** (2000) 295.
[8] FUJISAWA, A., et al., “Dynamic behavior of potential in the plasma core of the CHS heliotron / torsatron”, Phys. Rev. Lett. **79** (1997) 1054.
[9] FUJISAWA, A., et al., “Discovery of electric pulsation in a toroidal helical plasma”, Phys. Rev. Lett. **81** (1998) 2256.
[10] SHIMOZUMA, T., et al., “ECH system and its application to long pulse discharge in large helical device”, Fusion Eng. Design **53** (2001) 525.
[11] NARIHARA, K., et al., “Design and performance of the Thomson scattering diagnostic on LHD ”, Rev. Sci. Instr. **72** (2001) 1122.
[12] NAGAYAMA, Y., et al., ”Electron cyclotron emission diagnostics on the large helical device”, Rev. Sci. Instr. **70** (1999) 1021.
[13] SHAING, K.C., et al., “Plasma and momentum transport processes in the vicinity of a magnetic island in a tokamak”, Nucl. Fusion **43** (2003) 258.
[14] TODA, S., et al., “Theoretical study of the hysteresis characteristic of electric fields in helical plasmas”, Plasma Phys. Control. Fusion **43** (2001) 629.
[15] ESTRADA, T., et al., “Transient behaviour in the plasma core of TJ-II stellarator and its relation with rational surfaces”, Plasma Phys. Control. Fusion 44 (2002) 1615.